Journal of Structural Geology 33 (2011) 1406–1416

Contents lists available at ScienceDirect

Journal of Structural Geology

journal homepage: www.elsevier.com/locate/jsg

Fold geometry toolbox – Automated determination of fold shape, shortening, and material properties☆

Marta Adamuszek*, Daniel Walter Schmid, Marcin Dabrowski

Physics of Geological Processes, University of Oslo, 0316 Oslo, Norway

ARTICLE INFO

Article history:
Received 2 March 2011
Received in revised form
31 May 2011
Accepted 14 June 2011
Available online 28 June 2011

Keywords:
Fold shape analysis
MATLAB
Arclength
Amplitude
Wavelength
Thickness

ABSTRACT

The Fold Geometry Toolbox (FGT) provides a quick and quantitative shape analysis of generic, two-dimensional single and multilayer fold trains. Fold geometry is described using four basic parameters: fold arclength, amplitude, wavelength, and thickness. Several existing definitions of these parameters are implemented and in the case of thickness a new one is proposed. The advantage of FGT over existing tools is that it uses normalized and parameterized data representations, which ensure that the outcome of the analysis is invariant to rigid-body motions and dilation. FGT can deal with noisy interfaces and implements a new combination of filters that automates the identification of hinges and inflection points, minimizing the user input. In the final step of the analysis, FGT relates the obtained geometry parameter values to mechanical properties and shortening of folded layers. We demonstrate the use of FGT with data from a finite element simulation and a natural case. FGT is open source, written in MATLAB, and comes with a graphical user interface.

1. Introduction

The notion that a relationship exists between fold shapes, material properties, and driving forces goes back to the very beginning of structural geology. Already in the early nineteenth century Sir James Hall devised analogue and thought experiments to explain the mechanism that formed the folds in the southern Uplands of Scotland (Hall, 1815). For the case of a single layer, Biot (1957) and Ramberg (1963) analytically studied the relationship between the ratio of layer and matrix material properties and the ratio of dominant wavelength (L_d) to thickness (T) for linear viscous and elastic materials. Fletcher (1974) and Smith (1977) derived the corresponding expression for a non-linear viscous rheology. These analytical solutions are only valid for infinitesimal interface perturbations and L_d/T must be adjusted for both shortening and layer thickening (Sherwin and Chapple, 1968; Fletcher and Sherwin, 1978). Subsequently, a method to estimate bulk shortening and material property ratio from large amplitude fold shapes was developed by Schmalholz and Podladchikov (2001) based on theoretical considerations and numerical experiments.

The description of fold shape in two dimensions exploits various geometry descriptors as well as signal processing tools (e.g., Stabler, 1968; Hudleston, 1973; Twiss, 1988). Recent contributions include Bézier curves, conic sections, power functions, and superellipses (e.g., Bastida et al., 1999, 2005; Aller et al., 2004; Srivastava and Lisle, 2004; Lisle et al., 2006; Liu et al., 2009b). However, the mechanical theory of folding only links to a simple set of parameters describing fold geometry: fold arclength, amplitude, wavelength, and thickness. To enable the analysis of fold characteristics in the context of fold mechanics, it is crucial that these four parameters can be determined accurately, objectively, and fast. Consequently, we developed the fold geometry toolbox (FGT). FGT is an open source MATLAB application with a graphical user interface that largely automates fold characterization in two dimensions. No component of FGT is in itself pioneering, but rather the focus was to create a tool that fulfills the following conditions: (1) capable of dealing with generic fold shapes and noisy interfaces, (2) minimal operator bias (Chadwick, 1975), (3) invariant to rigid-body movement.

2. Fold geometry parameters

A fold is confined between two inflection points, i.e. the points where the interface curvature changes its sign. The point of local extremum of curvature is called the hinge. The fold geometry parameters of interest in our study are: fold arclength (L), amplitude (A), wavelength (λ), and thickness (h). The literature only

☆ FGT can be downloaded from the MATLAB file exchange.

* Corresponding author.
E-mail address: marta.adamuszek@fys.uio.no (M. Adamuszek).

0191-8141/$ – see front matter © 2011 Elsevier Ltd. All rights reserved.
doi:10.1016/j.jsg.2011.06.003

provides an unambiguous definition for the arclength. We therefore review the various definitions of other parameters and examine their a) unambiguity, b) applicability to generic fold geometries, and c) independence of coordinate system choice. Based on this analysis, we select the definitions that we implement in FGT. Note that the employed definitions of a fold only refer to a single interface of a layer, because it is not possible to ensure corresponding inflection and hinge points exist on the two interfaces of a layer. The exception is thickness, which is described below.

2.1. Arclength

The arclength s is the least disputed parameter because it is simply the interface length between two points (t_1 and t_2) on it. Using a parametric representation where interface point coordinates x and y are functions of parameter τ

$$s = \int_{t_1}^{t_2} \left(x'(\tau)^2 + y'(\tau)^2\right)^{1/2} d\tau \quad (1)$$

where the prime denotes the first derivative with respect to τ. Note that "fold arclength" L is actually twice the arclength between two inflection points. The reason for this modification is that fold arclength is used here in conjunction with wavelength, which refers to the full period.

2.2. Amplitude

Fold amplitude has been defined as:

A. The distance between the line joining two inflection points and the extremity of the fold (Ramsay and Huber, 1987).
B. The distance from the hinge to the line joining two inflection points (Park, 1997).
C. The distances between the inflection points and the line tangent at the hinge (Hudleston, 1973). In FGT, we use the average of these two values.
D. The distance between the median trace and the fold hinge (Price and Cosgrove, 1990).
E. The distance between the median trace and the hinge point measured along the axial trace (Davis and Reynolds, 1996; Twiss and Moores, 2007).
F. Half of the limb height measured parallel to the axial trace (Matthews, 1958).
G. Half the distance between two enveloping surface traces defined perpendicular to these interfaces (Turner and Weiss, 1963).
H. Half of the vertical hinge distance (Schmalholz, 2006).
I. Half of the height measured from crest to trough (van der Pluijm and Marshak, 2004).

These amplitude definitions are applied to a synthetic fold and analysed in Fig. 1. We abandon definitions D, E, F, and G due to the

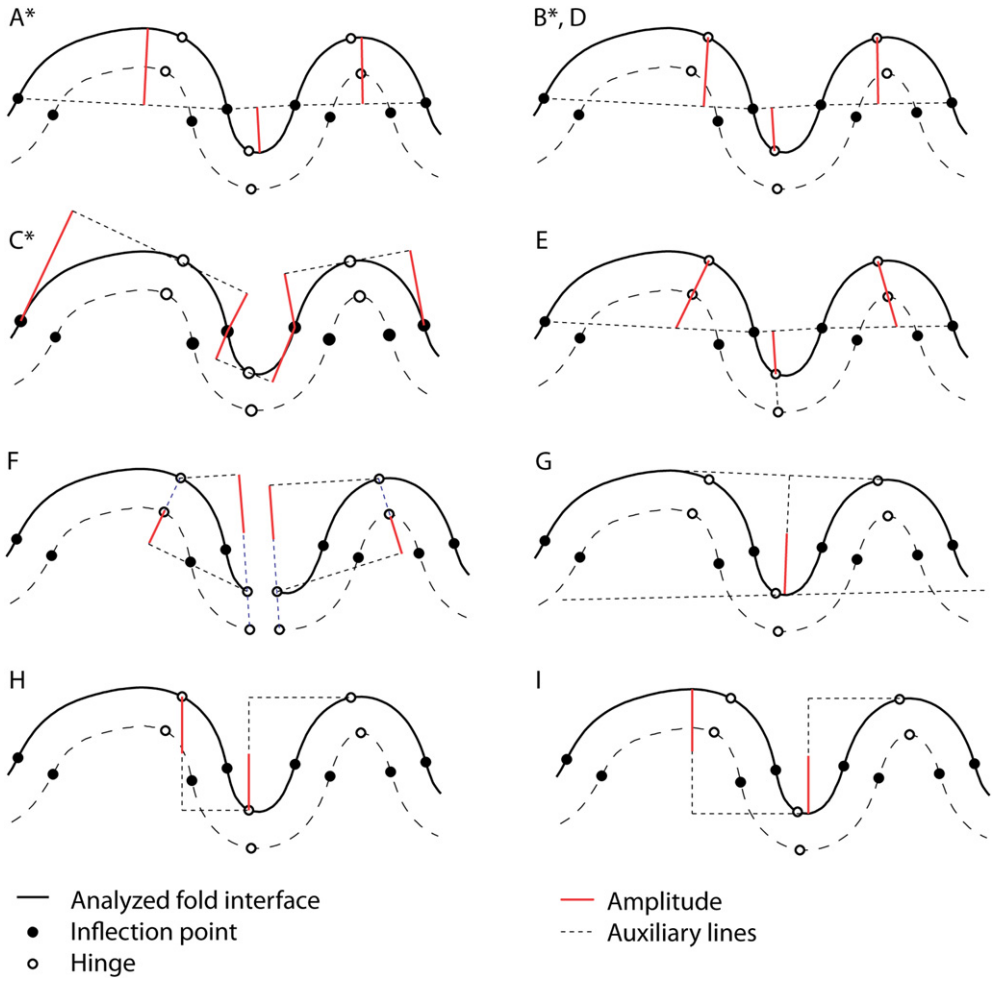

Fig. 1. Amplitude definitions applied to a synthetic fold. Letters A to I correspond to the definitions listed in section 2.2. * indicates methods implemented in FGT.

lack of precision in the description of the traces of median, axial, and enveloping surfaces. The median surface trace refers to the interface that joins the inflection points without specifying the shape in between these points (e.g., Twiss and Moores, 2007). We use a piecewise linear curve (Fig. 1D and E), which causes the definitions B and D to coincide. The axial surface trace refers to the interface that joins hinges on adjacent fold surfaces without describing the exact shape in between (e.g., Twiss and Moores, 2007). We use a straight line representation (Fig. 1E and F). Similarly, the enveloping surface trace, which is defined as the interface that bounds the fold train, lacks a shape description (e.g., Twiss and Moores, 2007). The enveloping surface trace in Fig. 1G is presented as the tangent to two alternating folds. Definition G is ambiguous as the two enveloping surface traces need not be parallel. Thus, in Fig. 1G we plot the amplitude along the line perpendicular to one enveloping surface trace only. Definitions H and I are not invariant with respect to rotation and therefore discarded. Consequently, only A, B, and C are used in FGT.

2.3. Wavelength

The wavelength of a fold is described as (Fig. 2):

A. Twice the distance between adjacent inflection points (Ramsay and Huber, 1987; Price and Cosgrove, 1990).
B. The distance between alternating hinges (van der Pluijm and Marshak, 2004). The method is applicable only to fold train that consists of more than three folds. In FGT, we use the average value if more than one wavelength can be constructed for a specific fold.
C. Four times the distance between the hinge and the point on the tangent at the hinge that has the shortest distance to the adjacent inflection points (Hudleston, 1973). For each fold, the average value of the two wavelengths is used in FGT.
D. The distance between alternating inflection points (Price and Cosgrove, 1990). We use the average of two values that correspond to one fold.
E. The horizontal hinge distance (Schmalholz, 2006).
F. Twice the axial trace separation measured perpendicular to axial trace (Matthews, 1958)
G. The distance between inflection points measured along the median trace (Davis and Reynolds, 1996).
H. The distance between geometrically similar points on alternating folds measured parallel to the median trace (Twiss and Moores, 2007).

E is discarded because it is not invariant with respect to rotation. F, G, and H are abandoned due to ambiguous median and axial surface trace definitions. Since axial traces are not parallel, definition F is represented by two lines, each perpendicular to one axial trace. Assuming piecewise linear median surface traces, A and G coincide. For general fold shapes, H only works for inflection points, which again results in A. Hence, four definitions, A, B, C, and D, fulfill our criteria and are implemented in FGT.

2.4. Thickness

We found two definitions of fold thickness (Fig. 3):

A. The distance between the fold interfaces, measured perpendicular to one interface (Sherwin and Chapple, 1968).
B. The distance between two parallel lines tangent to the upper and lower fold interface (dip-isogon method, Ramsay, 1967) measured either parallel to the axial plane or perpendicular to the constructed lines.

A1 and A2 in Fig. 3 illustrate the problems with definition A, because the thicknesses from using the lower and upper interface

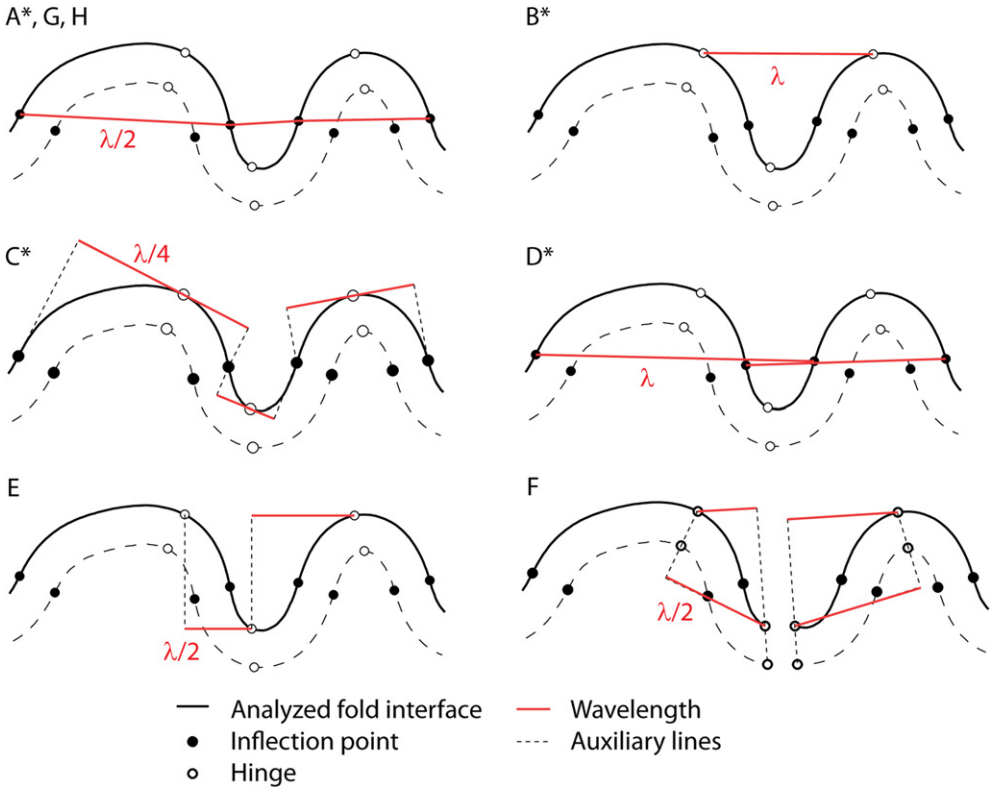

Fig. 2. Wavelength definition application to a synthetic fold. Letters A to H correspond to the definitions in section 2.3. * indicates methods implemented in FGT.

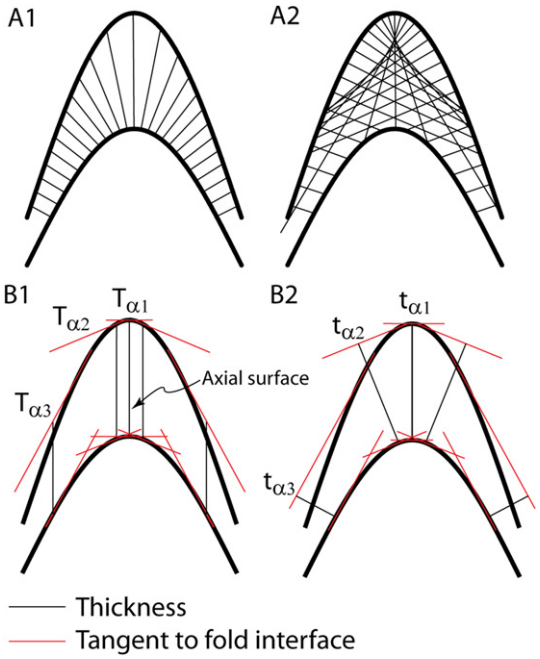

Fig. 3. Application of thickness definitions. A1 Thickness measured perpendicular to the bottom interface. A2 Thickness measured perpendicular to the top interface. B1 Thickness measured between set of two parallel lines tangent to the upper and lower interface and parallel to the axial surface (T_α). B2 Thickness measured as a distance between parallel lines tangent to the upper and lower interface (t_α).

are different. The latter case also results in lines originating from the hinge region that are sub-parallel to the limbs. For the dip-isogon method, the thickness defined parallel to the axial surface is inaccurate due to imprecise definition of the axial surface (Fig. 3). It also produces thickness lines that approach the orientation of the fold limbs. Definition B clearly overestimates the expected fold thickness. Furthermore, B is not applicable to generic fold shapes as noise and complex geometries may prevent the identification of meaningful pairs of tangents.

We suggest two alternative methods for calculating fold thickness. If only the average thickness of an entire fold train is required, one can measure the layer area and divide by the average arclength of the two interfaces (Fig. 4). However, the average value of an entire train may not be representative for individual folds. The second approach defines the thickness of individual folds, which we later refer to as a "local thickness". The fold train is divided into discrete folds based on the solution of Laplace's equation

$$\nabla^2 \Phi = 0 \tag{2}$$

with the following boundary conditions

$$\begin{aligned} \Phi &= 0 \; on \; \partial\Omega_L \quad \frac{\partial \Phi}{\partial n} = 0 \; on \; \partial\Omega_T \\ \Phi &= 1 \; on \; \partial\Omega_R \quad \frac{\partial \Phi}{\partial n} = 0 \; on \; \partial\Omega_B \end{aligned} \tag{3}$$

$\partial\Omega_T$ and $\partial\Omega_B$ are the upper and lower fold interface, respectively, and $\partial\Omega_R$ and $\partial\Omega_L$ represent the left and right fold boundary,

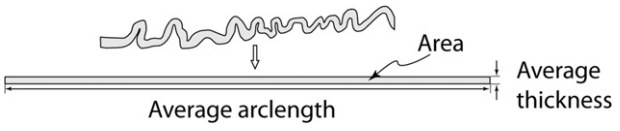

Fig. 4. Average thickness calculated as a ratio of the area between two interfaces and the average arclength.

constructed by connecting the fold interfaces. We obtain the solution using a finite element method solver (MILAMIN by Dabrowski et al., 2008) (Fig. 5A).

Due to the zero-flux boundary conditions, these contours are everywhere orthogonal to the fold interface. The iso-contours allow the finding of a set of analogous points on both interfaces, and thus facilitate a division of the fold train into separate folds. As by definition folds are limited by inflection points, the values Φ at these points should define the fold domain boundaries inside the layer. The corresponding points are identified on both interfaces and connected with a straight line. Since the inflection points on the upper and lower interface do not lie on the same iso-contour (Fig. 5A), the fold division is made separately based on the lower and upper interface (Fig. 5B and C). For each fold, the thickness is calculated by dividing the segment area by the average segment arclength.

3. Curvature, inflection points, and hinges

3.1. Parametric curvature

Curvature K is a measure of the interface deviation from being straight. We employ the parametric form of curvature to satisfy our criteria that the FGT measures work for arbitrary shapes and are invariant to rotation:

$$K = \frac{x'y'' - y'x''}{\left(x'^2 + y'^2\right)^{3/2}} \tag{4}$$

3.2. Discrete curvature

The discrete curvature calculation inside FGT operates on irregularly spaced input data. The technique approximates the derivatives by calculating the derivatives of a polynomial that locally interpolates between data points (e.g. Hildebrand, 1987). The order of the polynomial can be chosen to fit the data exactly or it can be lower and essentially acts as a low-pass filter. These two methods are used in FGT. The user can fit a second-order polynomial to the parameterized x and y coordinates of sets of three, five, or seven points. Here, the choice of three points results in the exact fit of the polynomial, whereas the other two options employ

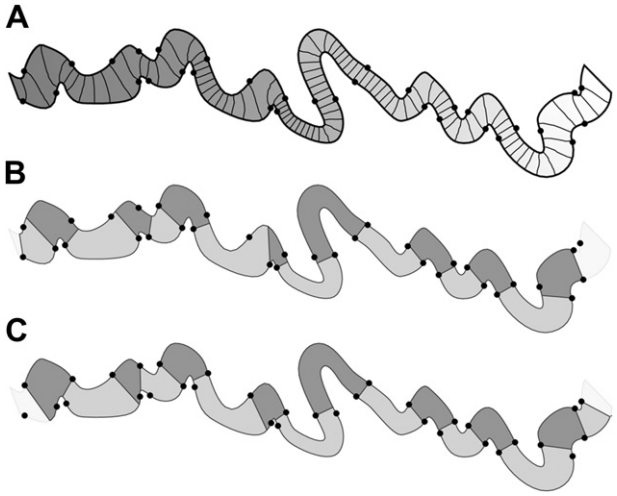

Fig. 5. Local thickness based on the solution of Laplace's equation. A) Iso-contours Φ are used to identify corresponding points on two fold interfaces. B) Division of folds based on the location of inflection points on the lower interface. C) Division of folds based on the location of inflection points on the upper interface.

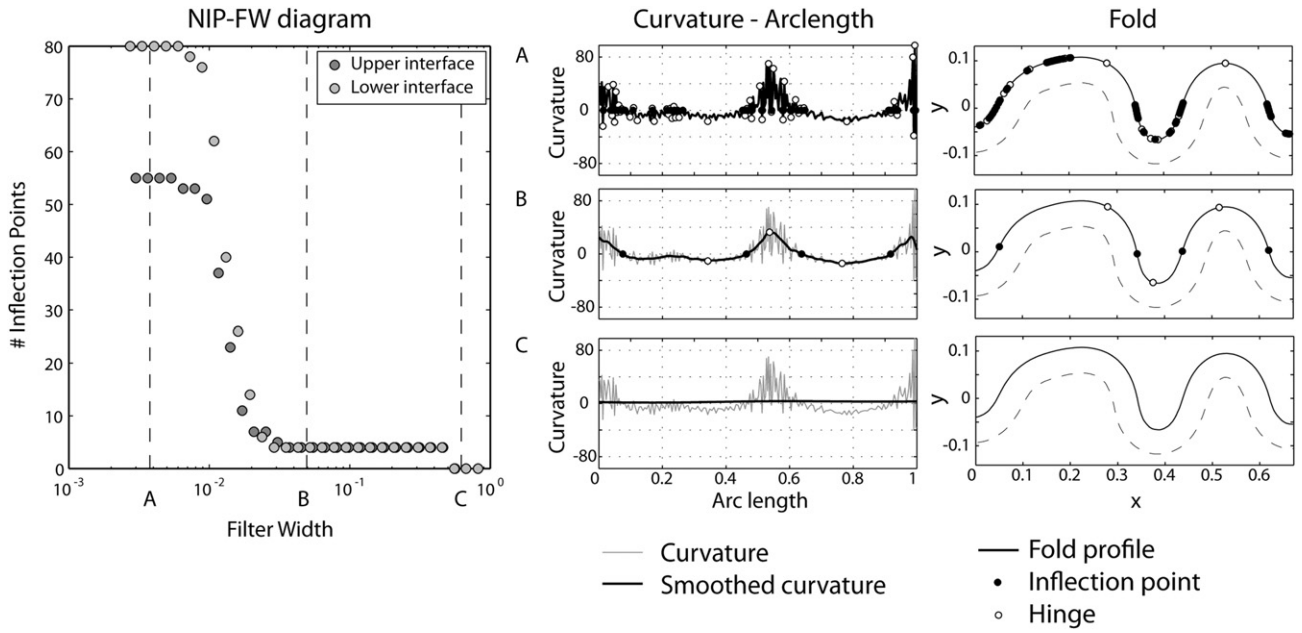

Fig. 6. Effect of Gaussian smoothing using different filter width on the curvature and number of detected inflection points.

the low-pass filter. The derivatives are evaluated at the central point. In case of nodes so close to the boundary that their curvature calculation would require points outside the domain, the polynomial is fitted to the marginal set of points and the derivatives calculated for the respective points. Fitting a second-order polynomial to a set of five or seven points is only recommended for folds with poor shape approximations such as stair-step like interface shapes that may result from pixel image digitization.

3.3. Curvature smoothing

Natural folds rarely have smooth interfaces and additional noise may be introduced by the digitization process. The resulting discrete curvature can be noisy and cause detection of a large number of false hinges and inflection points (Fig. 7A). We employ a Gaussian filter to reduce curvature oscillations. This filter is a weighted, moving average method, where the value in each data point is replaced by the weighted average of values within the smoothing window of size Ψ. The smoothed curvature in a point s_j is

$$\tilde{K}(s_j) = \frac{\sum_{i=1}^{n} w_i \cdot K(s_i)}{\sum_{i=1}^{n} w_i} \tag{5}$$

The weights w_i are evaluated based on the arclength between points s_i and s_j:

$$w_i = \frac{1}{\sqrt{2\pi\sigma^2}} e^{-(s_i - s_j)^2/2\sigma^2} \tag{6}$$

where the standard deviation σ is set to $\psi/6$ This method is suitable for irregularly spaced data and allows for any number of data points within the filter window.

The amount of smoothing and consequently the number of detected hinge and inflection points is controlled by the width of the smoothing filter. The filter width is not a priori known and must be user specified. To facilitate this selection, we systematically scan through the possible range of filter widths, i.e. from the shortest distance between the input points to the arclength of the entire fold train, and analyse the number of resulting inflection points. Plotting the number of inflection points versus the filter width results in a NIP-FW (Number of Inflection Points - Filter Width) diagram. On this diagram plateaus correspond to folds on different scales. Some plateaus may represent true folds while others would usually be classified as noise. Since this distinction is somewhat arbitrary and application specific, we let the user make this choice.

For a chosen filter width, the FGT plots original and smoothed curvature versus arclength, including the detected hinge and inflection points. These points are also plotted on the actual fold interfaces. This procedure allows for quick determination of the suitable smoothing filter width (Fig. 6). The NIP-FW shows five regimes of alternating plateaus and ramps. The plateau at small filter width is due to the presence of small-scale perturbations that are larger than the smallest point distance (Fig. 6A). Large filter widths smooth these perturbations and progressively decrease the number of inflection points, represented by a ramp on the NIP-FW. The second plateau appears when the filter size is large enough to smooth the noise but too small to affect the fold shape (Fig. 6B). Choosing a filter width from this plateau results in the most favorable inflection point detection. A further increase of the filter width causes over-smoothing of the curvature, which results in a decrease of the number of inflection points towards zero (Fig. 6C).

3.4. Inflection points

Even after the application of a reasonable smoothing window, the number of detected inflection points may not be satisfactory (cf. Fig. 7A and B). This can be caused by interface segments that are almost straight and show small curvature variations around zero. In FGT, we only consider folds with considerable arclength and curvature. The selection criterion is the integral of the absolute curvature along the arclength between inflection points. If an individual value is smaller than a certain percentage, by default set to 10%, of the average of all values then the curvature between the corresponding inflections is set to zero. If the curvature changes

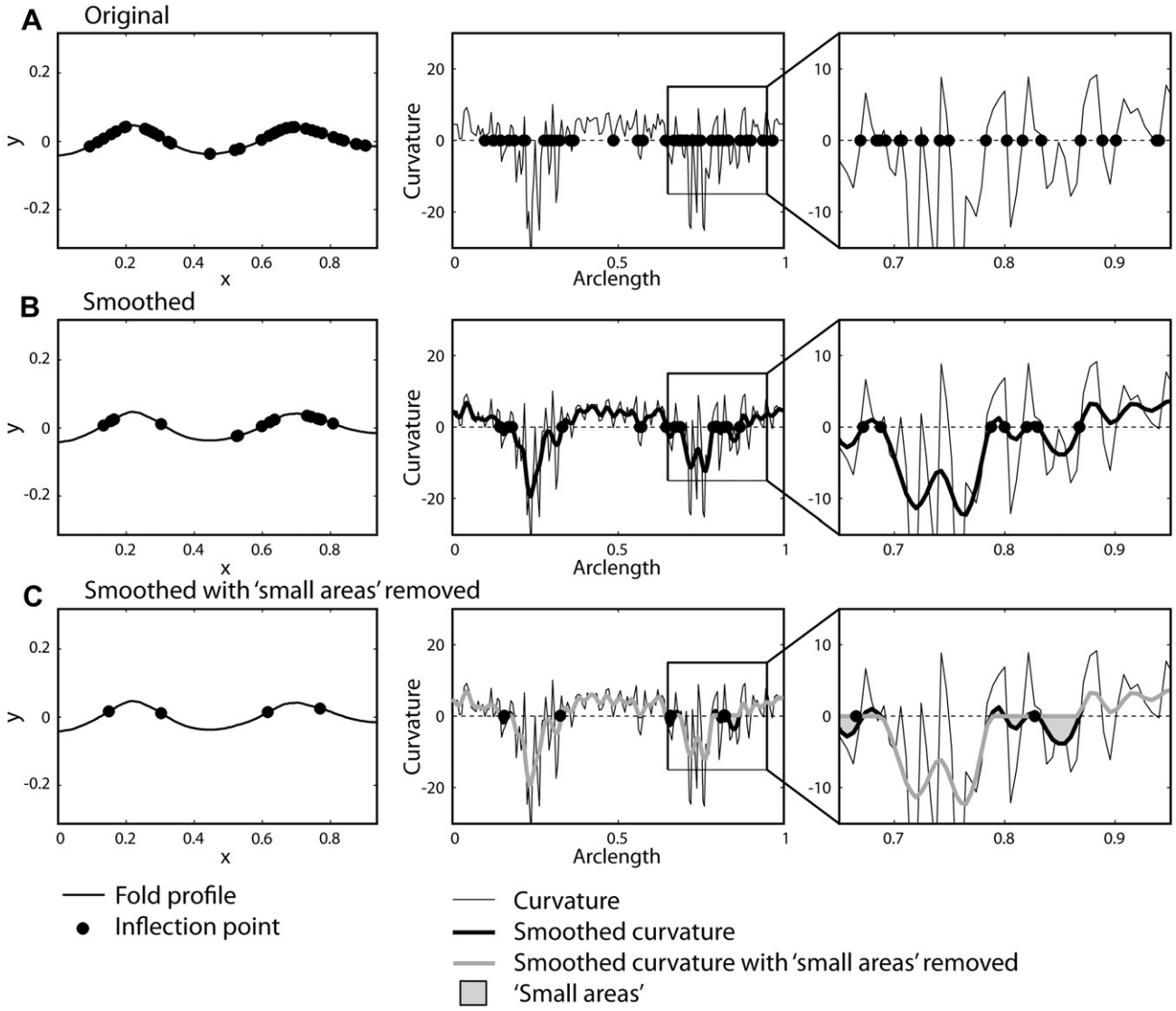

Fig. 7. Curvature and resulting inflection points. A) Original curvature. B) Smoothed curvature. C) Smoothed curvature with the 'small areas' removed.

sign around this segment, we place an inflection point at its middle (Fig. 7C).

3.5. Hinges

A hinge is the point of local extremum of curvature between two inflection points. This criterion is employed as the standard method in the FGT. This definition fails for concentric folds, where the curvature is constant. To deal with such cases, FGT provides a second, user selectable, method of hinge positioning whereby all points in curvature-arclength space between inflection points are fitted to a second-order polynomial. The local extremum of this polynomial represents the hinge.

Cases with multiple local extrema of curvature may occur and are, in fact, common due to noise. With the exception of perfect, synthetically generated box folds, it is unlikely that several such hinges have exactly the same curvature value. Furthermore, no definition for amplitude or wavelength deals with multiple hinges (see section 2.2 and 2.3). Therefore, FGT detects only one hinge per fold, i.e. the one characterized by the highest absolute value of curvature.

4. Estimation of material properties and shortening

In the final step of the FGT analysis, we provide estimates of shortening and material properties, using a variety of analytical and numerical approaches. The analytical solutions include thin-plate analysis of folding of elastic and viscous layers (Biot, 1961, 1965; Ramberg, 1961; Currie et al., 1962; Fletcher, 1974) and the thick-plate solution for viscous single layer folds (Fletcher, 1977). We also include methods that consider finite strain (Sherwin and Chapple, 1968; Fletcher and Sherwin, 1978; Schmalholz and Podladchikov, 2001).

Methods that are not corrected for finite strain require the initial (infinitesimal amplitude) fold wavelength to thickness ratio. As a proxy, we use the final fold arclength to thickness ratio (L/h) (Sherwin and Chapple, 1968). In FGT, L/h is calculated per fold train as the ratio of average fold arclength to average thickness. Note that in FGT all means are arithmetic means and ratios are those ratios of already averaged values. The only exception is the method by Fletcher and Sherwin (1978), where the ratios computed for individual folds are used.

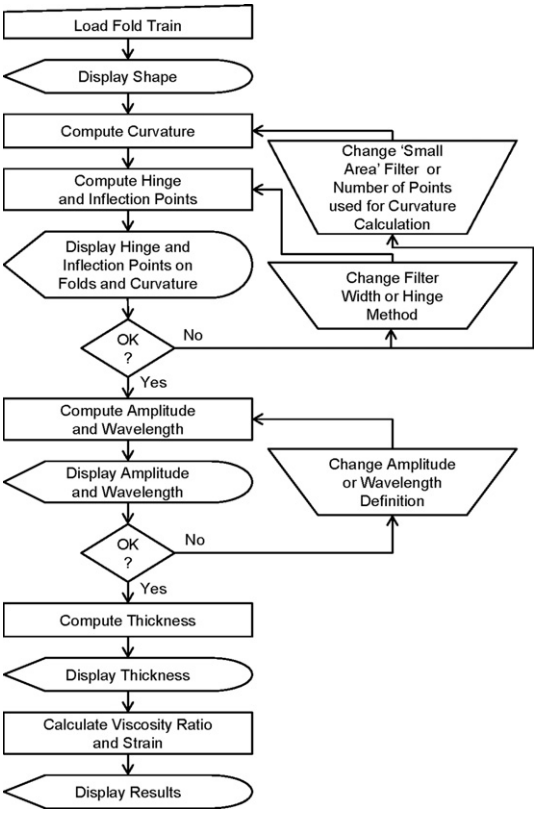

Fig. 8. FGT flow chart.

5. Flow chart

FGT is used to perform the following tasks (Fig. 8):

i. Load Fold Train.

Three different input types can be processed. 1) MATLAB files that contain a fold train structure (see Appendix A). 2) Scalable vector graphics (SVG) files that contain the result of an image digitization in a vector graphics program (see Appendix B). 3) Images of folds. In the last case, FGT provides a tool for digitization. However, the capabilities of method 3 are minimal and we suggest option 2 instead. All length measurements are normalized by the arclength of the first fold interface.

ii. Compute and Smooth Curvature.

The parameterized curvature is calculated based on second-order polynomials that are locally fitted, by default, to a set of three points. The effect of curvature smoothing using a Gaussian filter is tested, where for 30 different filter widths the number of inflection points is determined. A diagram of filter width and corresponding number of inflection points is produced (NIP-FW diagram). The curvature is initially smoothed with a default filter width of 0.01 and the inflection points are identified. Folds are eliminated that have a product of average curvature and arclength below a certain percentage, by default set to 10%, of its mean value ('small area' filter). Finally, only one hinge point is determined for each fold. The hinges and inflection points are plotted on the fold and the curvature plots.

The user can change: a) filter width, b) number of points based on which the curvature is calculated, c) 'small area' filter, and d) hinge method.

iii. Compute Amplitude and Wavelength.

Based on the detected hinges and inflection points, amplitude and wavelength are determined using methods described in sections 2.2 and 2.3. The average value is calculated.

iv. Compute Thickness.

Local and average thickness are calculated. The fold train is divided into individual folds. The values of the average thickness and average local thickness are compared.

v. Determine shortening and material properties.

The geometrical parameters are used to calculate shortening and material parameters.

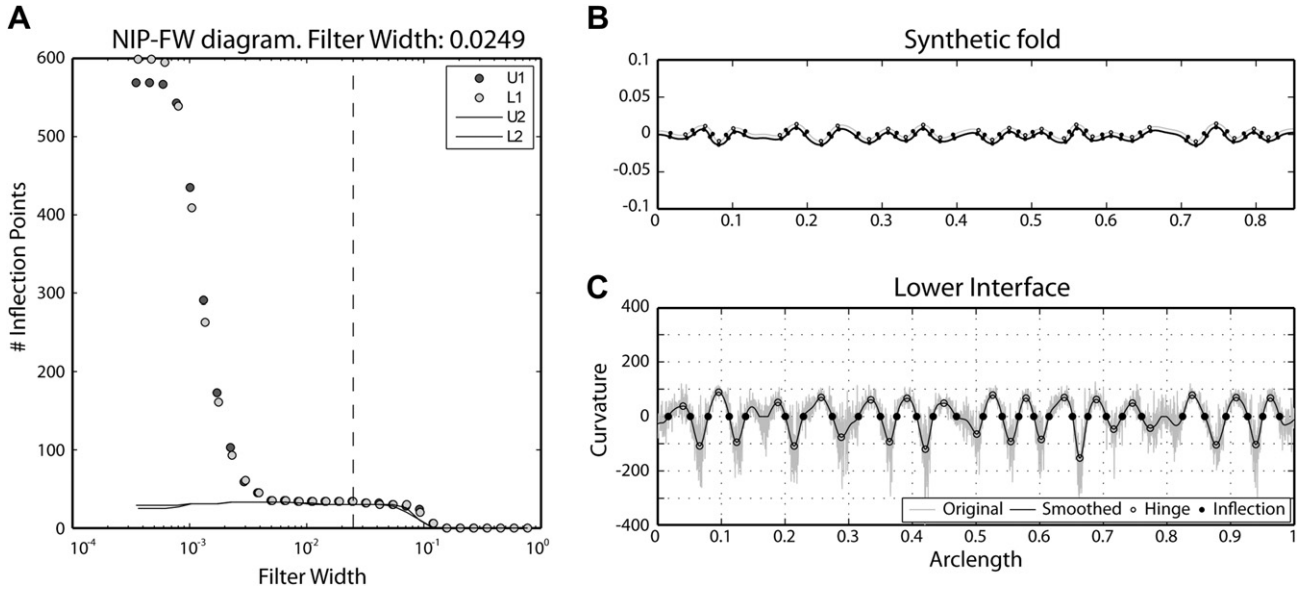

Fig. 9. A) NIP-FW plot with a selected filter width. The circles show the relation between the number of inflection points and filter width after applying a Gaussian filter on the upper (U1) and lower interface (L1) and the solid lines show the additional influence of the 'small area' filter (U2 and L2). B) Fold interface with identified hinges and inflection points. C) Original and smoothed curvature with identified hinges and inflection points.

Table 1
Data for the single layer synthetic fold train normalized by the arclength of the lower fold interface. The data from both interfaces are processed together. The letters below the parameters correspond to the definitions of amplitude, wavelength, and thickness presented in section 2. With the exception of the ratios, all actual values are multiplied by 1000.

Parameter	Mean value	Min	Max	Standard deviation
L-Arclength	66.1	42.8	137	20.4
A-Amplitude				
A	7.33	3.18	12.2	2.03
B	7.12	3.15	11.8	1.93
C	7.90	3.21	14.5	2.67
λ-Wavelength				
A	56.3	32.4	129	20.2
B	55.4	37.8	87.3	12.4
C	55.3	32.3	120	18.3
D	56.0	42.8	87.2	11.6
h-Thickness				
A	5.02	4.94	5.09	0.0365
B	5.03	–	–	–
$\langle L\rangle/\langle h\rangle$	13.2	–	–	–
L/h	13.2	8.50	27.1	4.02

6. Examples

We successfully tested the FGT on a range of natural and synthetic folds, and we provide the corresponding data files together with FGT for download. In this section, we present two cases: i) a synthetic single layer and ii) a natural two-layer fold train.

6.1. Synthetic fold train

A synthetic fold train (Fig. 9) is obtained by applying the finite element method code MILAMIN (Dabrowski et al., 2008) to shorten a single layer and its matrix. Both are linear viscous fluids, with the viscosity of the layer 100 times that of the matrix. The initial perturbation of the layer interfaces is a red-noise, whose maximum amplitude is 1/20 of the layer thickness. The layer and matrix are shortened by 30%. The model width is 20 times the expected dominant wavelength. The resulting folds exhibit shapes ranging from gentle and wide to open and broad with rounded hinge zones. The NIP-FW plot exhibits three distinct plateaus (Fig. 9A). The first plateau occurs due to the presence of noise, whereas the third one results from over-smoothing. The curvature is calculated based on a set of three points and smoothed using a filter width from the middle plateau (dashed line in Fig. 9A). The value of the 'small area' filter is set to 10%. Hinges are defined with the standard method. The identified hinges and inflection points are plotted on the fold interface and curvature, respectively (Fig. 9B and C).

Different definitions for amplitude and wavelength give overall comparable average values of around $7.5*10^{-3}$ and $5.6*10^{-3}$, respectively (Table 1) (all measurements are normalized by the arclength of the lower interface). The span of values is similar except for wavelength definitions A and C where higher variations are observed. The average thickness and averaged local thickness give similar values of $\sim 5*10^{-3}$. The variability of the local thickness is also small. The ratio of mean fold arclength to mean thickness is similar to the mean ratio of fold arclength to thickness, ~13.2.

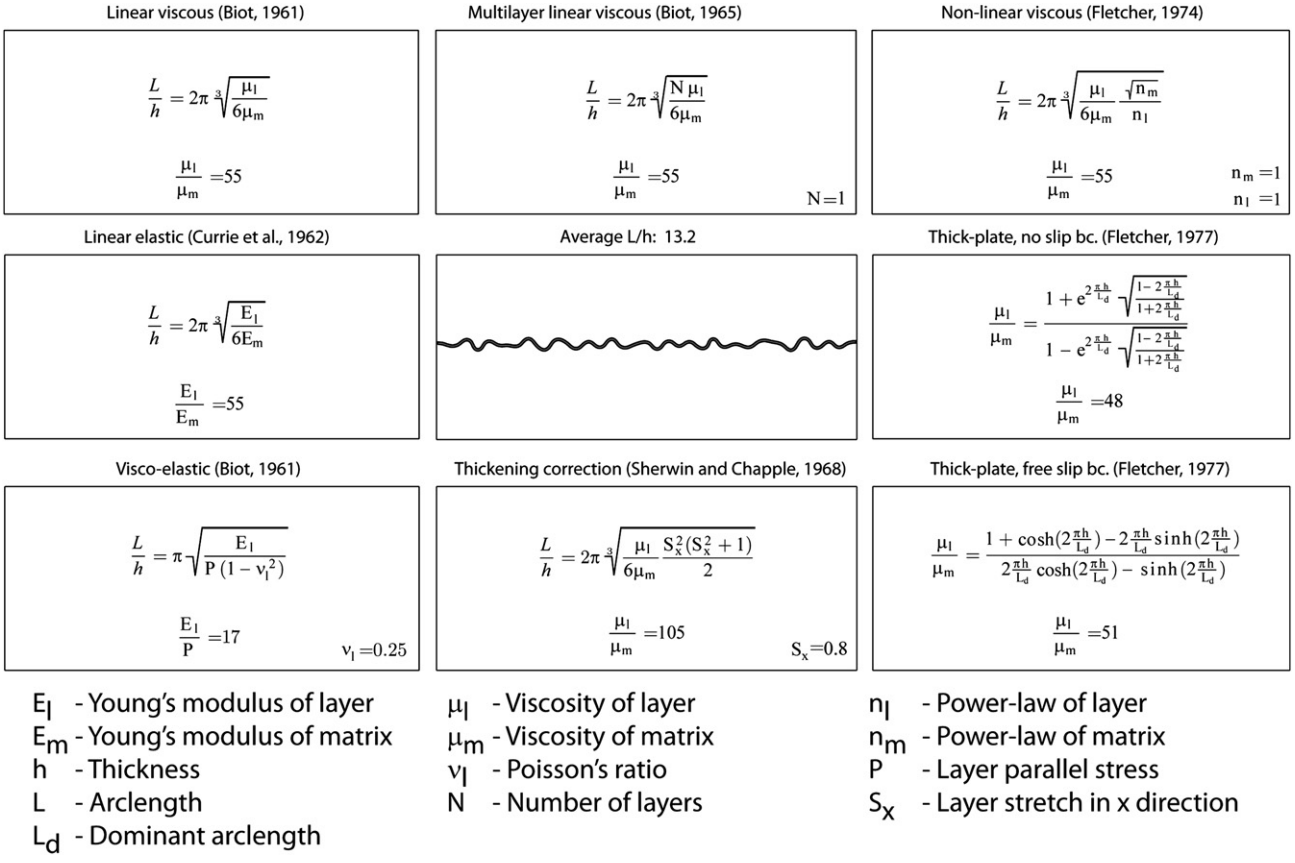

Fig. 10. FGT figure that shows the implemented solutions with the resulting values for the analysed synthetic fold.

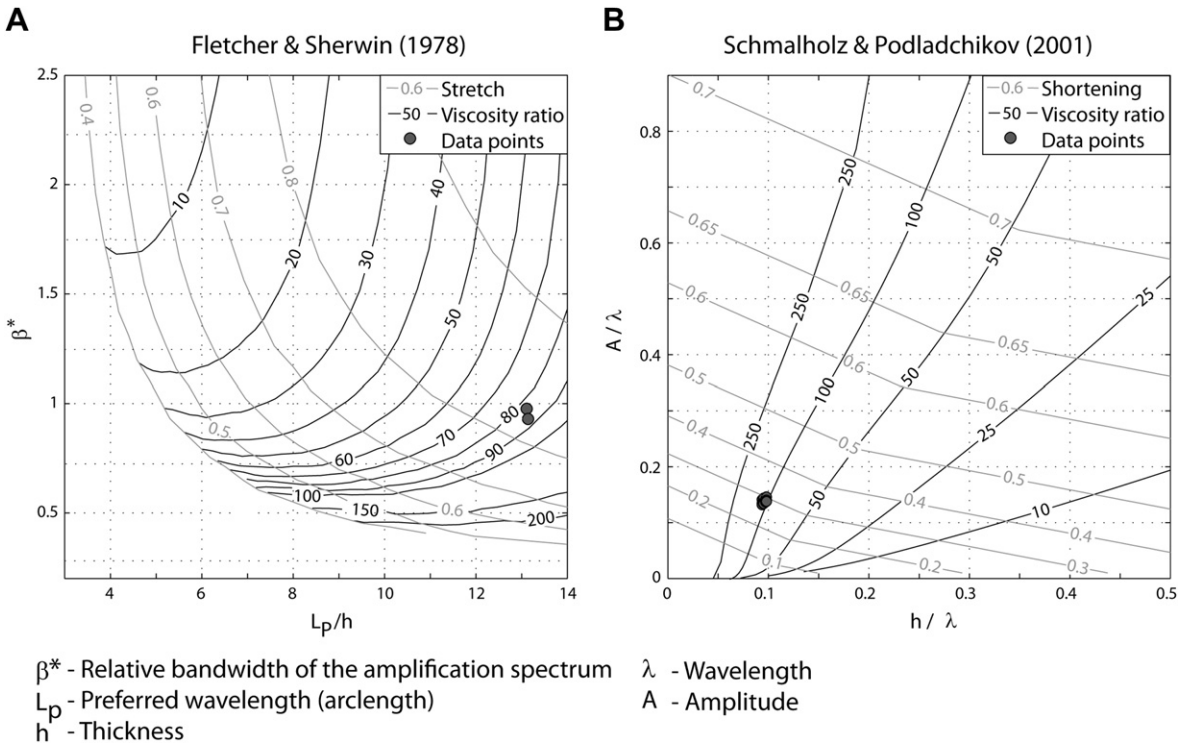

Fig. 11. Strain and viscosity ratio after A) Fletcher and Sherwin (1978) (two dots represent the values for upper and lower interfaces), and B) Schmalholz and Podladchikov (2001) (each dot represents a combination of various amplitude, wavelength, and thickness definitions for both upper and lower interfaces).

The values for fold arclength, amplitude, wavelength, and thickness are used to estimate the correspondence of the viscosity ratio and shortening. These estimates are compared with the actual values used to generate this synthetic model. The average arclength to thickness ratio of 13.2 results in viscosity ratio of 55 according to the thin-plate theory (Biot, 1961), and viscosity ratios of 48 and 51 according to the thick-plate theory (Fletcher, 1977) with no slip and free slip boundary conditions, respectively (Fig. 10). These values are substantially less than the actual viscosity ratio of 100. One reason for this mismatch is that finite strain is not considered. In this synthetic case, we have the advantage that we can directly determine the actual layer thickening, which was ~25%, equivalent to a layer-parallel shortening stretch of 0.8. Application of the corresponding correction for finite strain (Sherwin and Chapple, 1968) yields a viscosity ratio of 105, a much better match. The elastic, visco-elastic, multilayer and non-linear viscous relations in Fig. 10 are irrelevant for this model.

The method by Fletcher and Sherwin (1978) yields a viscosity ratio close to 85 (Fig. 11A), and indicates that the stretch at which wavelength selection took place is ~0.83. Using the method by Schmalholz and Podladchikov (2001), the average amplitude to average wavelength ratio and the average thickness to average wavelength ratio cluster in one spot, irrespective of definition, yielding an average viscosity ratio of ~100 and an average bulk shortening around 30% (Fig. 11B).

6.2. Natural fold train

A natural two-layer fold train (Fig. 12) is digitized using a vector graphics software and exported as an SVG file to FGT (Appendix B). The fold train has various fold shapes from wide and gentle to short and tight with sharp to rounded hinge zones. Some shapes approximate concentric folds while others resemble box folds. For this example, the seven point-based curvature computation in combination with a Gaussian filter width of around 0.0157 yields the most satisfactory results (Fig. 13A). The small area filter is set to 10%.

The mean fold arclength in both fold trains is approximately $35*10^{-3}$ (Table 2) (all measurements are normalized by the arclength of the lowermost interface). All definitions for the amplitude and wavelength give comparable average values for both interfaces of upper and lower layer equal to ca. $23*10^{-3}$ and $57*10^{-3}$, respectively. The data spans are again larger for wavelength definitions A and B. The fold is divided into individual folds, based on which the local thickness is calculated. The average layer thicknesses are around $8*10^{-3}$ and $8*10^{-3}$ for the upper and lower layer, irrespective of the method. The ratio of average fold arclength to average thickness is around 8 for the upper fold train and around 16 for the lower one. Using the expression for a multi-(two) layer by Biot (1965), we obtain a viscosity ratio with respect to the matrix of 53 for the upper and 6 for the lower layer. This difference in ratios

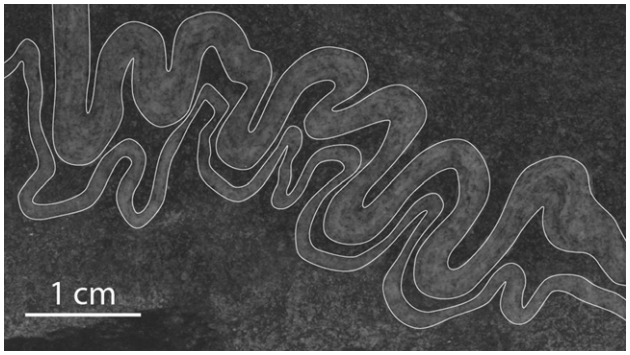

Fig. 12. Quartz-feldspar dominated layer embedded in a biotite rich matrix (Lavik, Norway).

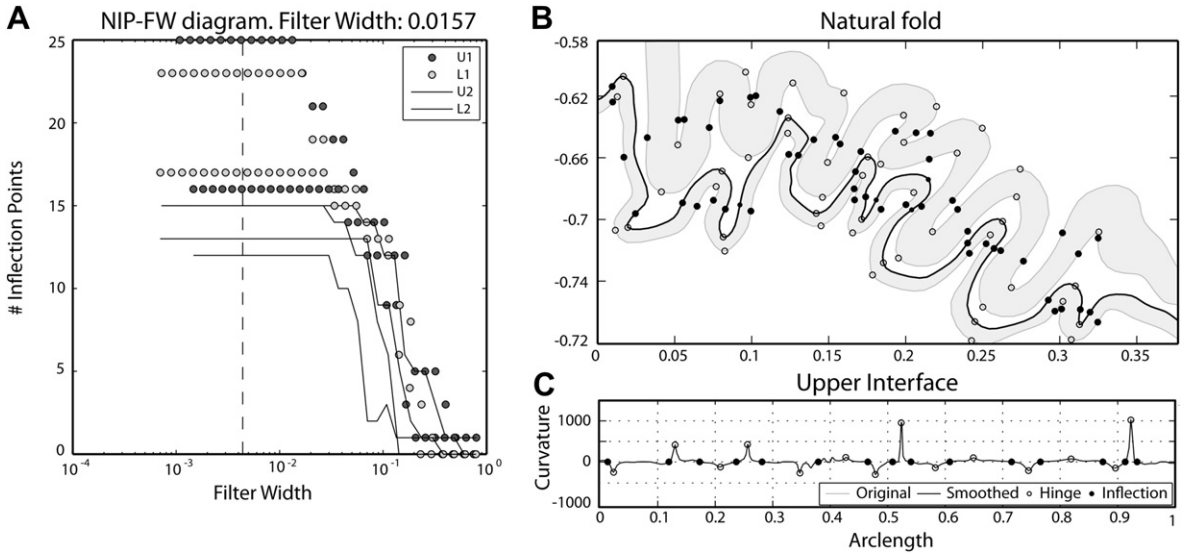

Fig. 13. A) NIP-FW plot with determined filter width. The circles show the relation between the number of inflection points and filter width after applying a Gaussian filter on the upper (U1) and lower interface (L1) and the solid lines show the additional influence of the 'small area' filter (U2 and L2). B) Fold interface with identified hinges and inflection points. C) Original and smoothed curvature with identified hinges and inflection points.

Table 2
Data for the natural multilayer fold train normalized by the fold arclength of the lowermost interface. The data from both interfaces of an individual layer are processed together. Upper and lower refer to the corresponding layers in the Fig. 12. Letters below the parameters correspond to the definitions of amplitude, wavelength, and thickness presented in section 2. With the exception of the ratios, all actual values are multiplied by 1000.

Parameter	Mean value		Min		Max		Standard deviation	
Fold	Upper	Lower	Upper	Lower	Upper	Lower	Upper	Lower
L-Arclength	141	130	27.2	27.5	246	269	67.7	70.5
A-Amplitude								
A	24.3	21.4	2.67	3.95	48.0	52.5	13.7	14.5
B	21.4	20.2	1.58	3.58	45.6	51.6	13.1	14.5
C	27.6	25.6	3.55	2.54	50.8	51.3	12.4	13.7
λ-Wavelength								
A	59.5	60.5	7.38	8.96	117	168	33.7	40.0
B	54.9	59.2	36.3	28.0	65.3	88.9	7.91	15.9
C	48.8	48.2	9.25	12.7	103	120	26.9	28.8
D	56.8	54.6	48.2	26.9	69.7	88.2	6.58	16.9
h-Thickness								
A	18.0	8.02	13.5	6.34	23.6	10.3	2.97	1.21
B	18.7	7.97	–	–	–	–	–	–
$\langle L\rangle/\langle h\rangle$	7.57	16.2	–	–	–	–	–	–
L/h	8.13	16.9	1.56	2.73	15.5	35.9	4.03	9.74

indicates that the fold development is controlled by the thicker upper layer and the lower one followed more or less passively. The other methods are ignored because they are unsuitable for the multilayer case.

7. Discussion and conclusions

FGT estimates material properties and amount of shortening from fold shape. Previously developed numerical tools for fold geometry analysis either have a different focus or fail to work for complex fold shapes, e.g. Isogon (Peña, 2001), FoldModeler (Bobillo-Ares et al., 2004), Fold Profiler (Lisle et al., 2006), and Bezier Fold Profiler (Liu et al., 2009a). Srivastava and Rastogi (2010) developed HingeInflex to numerically determine inflection and hinge points. Noise in the fold profile is reduced by fitting a polynomial of user-specified order to the fold interface. Unfortunately, HingeInflex is restricted to the analysis of fold shapes that can be described by a single-value function. While this limitation is not crucial for idealized low strain cases, the tool will fail for many natural cases such as shown in Fig. 12.

In FGT, only definitions and methods are implemented that are applicable to all fold shapes and invariant to rotation and dilation. The key element to achieve this implementation is the use of parametric curvature. Curvature noise is smoothed using a Gaussian filter in combination with the 'small area' filter. The choice of the filter width and size of the 'small area' has to be made by the user and is therefore biased. However, a reasonable range of parameters can be inferred from a NIP-FW diagram and the consequence of a particular choice is immediately computed, and the resulting hinge and inflection points plotted on the analysed fold train. Various definitions of amplitude, wavelength, and thickness are implemented so that the user can compare different approaches or choose the specific definition that is most suitable for the analysis of a particular fold train. Due to the lack of a robust thickness definition in the literature, we developed new definitions. If only the average thickness of an entire fold train is required, the area is divided by the average fold train arclength. If individual fold thicknesses are of interest, we partition the fold based on the solution of the Laplacian and position of inflection points. This measure is objective and reproducible.

The fold definition used in FGT, the segment of an interface between two inflection points, only refers to an interface and not a layer of finite thickness. This definition circumvents problems with inflection and hinge point mismatches on the two interfaces of a layer. Hence, the two interfaces are processed separately and all geometrical parameters are computed for every individual fold on an interface. The data from both interfaces are then used to compute fold train averages.

The fold geometry analysis in FGT is robust and works for generic fold shapes, including extremes such as circular fold trains. It is fast and easy to use via graphical user interface. However, quantifying fold geometry on its own is of limited interest. The natural example analysed in section 6.2 demonstrates only the applicability to complex fold shapes. The synthetic case, section 6.1, is an example of the applicability to derive viscosity ratios and shortening estimates. The estimation of the viscosity ratio based on

the analytical method provides a close result only for the Biot (1961) method with correction (Sherwin and Chapple, 1968). Also, both numerical methods developed by Fletcher and Sherwin (1978) and Schmalholz and Podladchikov (2001) approximate fairly accurately the shortening and material properties. More detailed work with synthetic models is required to study how initial noise, effective viscosity ratio, and shortening influence the reliability of the inferred estimates.

Acknowledgments

We acknowledge the Center of Excellence grant from the Norwegian Research Council to PGP (Physics of Geological Processes) at the University of Oslo. We are grateful to Ray Fletcher and Stefan Schmalholz for providing the codes for estimating shortening and viscosity ratio. We thank Espen Jettestuen, Jacqueline Reber, and Marcin Krotkiewski for many valuable suggestions. Furthermore, we are grateful to Peter J. Hudleston, Richard J. Lisle, and Bill Dunne for the comments on the manuscript.

Appendix A. Fold data structure

All fold data are stored in a single MATLAB structure array called *Fold*. Every entry in *Fold* has a field *Face* with two entries, corresponding to the upper and lower interface. Every entry in *Face* has two fields *X.Ori* and *Y.Ori* that contain the x and y coordinates of a single fold interface, respectively. If the input is specified as a MATLAB file then it must contain the structure *Fold*.

Appendix B. Picture digitization in adobe illustrator

(1) Import image. (2) Draw separate contours of the upper and lower interface using the *Pen Tool* (Bezier curve). In the case of a multilayer, draw each fold on the separate layers. (3) Add points on the curve with *Object/Path/Add more anchor points* to create around 20–40 points on the fold. (4) Use *Object/Path/Simplify* to produce straight lines between the points. (5) Save data as a SVG file.

References

Aller, J.D., Bastida, F., Toimil, N.C., Bobillo-Ares, N.C., 2004. The use of conic sections for the geometrical analysis of folded surface profiles. Tectonophysics 379 (1–4), 239–254.
Bastida, F., Aller, J., Bobillo-Ares, N.C., 1999. Geometrical analysis of folded surfaces using simple functions. Journal of Structural Geology 21 (7), 729–742.
Bastida, F., Aller, J., Bobillo-Ares, N.C., Toimil, N.C., 2005. Fold geometry: a basis for their kinematical analysis. Earth-Science Reviews 70 (1–2), 129–164.
Biot, M.A., 1957. Folding instability of a layered viscoelastic Medium under compression. Proceedings of the Royal Society of London Series A-Mathematical and Physical Sciences 242 (1231), 444–454.
Biot, M.A., 1961. Theory of folding of stratified viscoelastic media and its implications in tectonics and orogenesis. Geological Society of America Bulletin 72 (11), 1595–1620.
Biot, M.A., 1965. Theory of similar folding of first and second Kind. Geological Society of America Bulletin 76 (2), 251.
Bobillo-Ares, N.C., Aller, J., Toimil, N.C., Bastida, F., 2004. FoldModeler: a tool for the geometrical and kinematical analysis of folds. Computers & Geosciences 30, 147–159.
Chadwick, P.K., 1975. Psychological analysis of Observation in Geology. Nature 256 (5518), 570–573.
Currie, J.B., Patnode, H.W., Trump, R.P., 1962. Development of folds in sedimentary strata. Geological Society of America Bulletin 73, 655–674.
Dabrowski, M., Krotkiewski, M., Schmid, D.W., 2008. MILAMIN: MATLAB-based finite element method solver for large problems. Geochemistry Geophysics Geosystems 9.
Davis, G.H., Reynolds, S.J., 1996. Structural Geology of Rocks and Regions. John Wiley and Sons, Inc., New York. 776.
Fletcher, R.C., 1974. Wavelength selection in folding of a single layer with power-Law Rheology. American Journal of Science 274 (9), 1029–1043.
Fletcher, R.C., 1977. Folding of a single viscous layer: exact infinitesimal-amplitude solution. Tectonophysics 39, 593–606.
Fletcher, R.C., Sherwin, J.A., 1978. Arc lengths of single layer folds - Discussion of Comparison between theory and Observation. American Journal of Science 278 (8), 1085–1098.
Hall, J. Sir, 1815. On the vertical position and convolution of certain strata, and their relation with granite. Transactions of the Royal Society of Edinburgh 7, 79–108.
Hildebrand, F.B., 1987. Introduction to Numerical Analysis. Dover Publications, New York.
Hudleston, P.J., 1973. Fold Morphology and Some geometrical implications of Theories of fold development. Tectonophysics 16 (1–2), 1–46.
Lisle, R.J., Martinez, J.L.F., Bobillo-Ares, N., Menedez, O., Aller, J., Bastida, F., 2006. FOLD PROFILER: a MATLAB (R)-based program for fold shape classification. Computers & Geosciences 32 (1), 102–108.
Liu, C., Zhang, Y., Wang, Y., 2009a. Analysis of complete fold shape based on quadratic Bézier curves. Journal of Structural Geology 31 (6), 575–581.
Liu, C., Zhang, Y.K., Shi, B., 2009b. Geometric and kinematic modeling of detachment folds with growth strata based on Bezier curves. Journal of Structural Geology 31 (3), 260–269.
Matthews, D.H., 1958. Dimensions of Asymmetrical Folds Geological Magazine, 95, p. 511–513.
Park, R.G., 1997. Foundation of Structural Geology. Chapman and Hall, New York, 216 p.
Peña, J.M.V., 2001. Isogons: a program in pascal to draw the dip isogons of folds. Computers & Geosciences 27, 601–606.
Price, N.J., Cosgrove, J.W., 1990. Analysis of Geological Structures. Cambridge University Press, Cambridge.
Ramberg, H., 1961. Contact strain and fold instability of a multilayered body under compression. Geol. Rund. 51, 405–439.
Ramberg, H., 1963. Fluid dynamics of viscous buckling applicable to folding of layered rocks. Bull. Am. Ass. Petr. Geol 47 (3), 484–505.
Ramsay, J.G., 1967. Folding and Fracturing of Rocks. Mc-Graw Hill, New York, 568 p.
Ramsay, J.G., Huber, M.I., 1987. Folds and Fractures. Modern Structural Geology, vol 2. Academic Press, London, 700 p.
Schmalholz, S.M., 2006. Scaled amplification equation: a key to the folding history of buckled viscous single-layers. Tectonophysics 419 (1–4), 41–53.
Schmalholz, S.M., Podladchikov, Y.Y., 2001. Strain and competence contrast estimation from fold shape. Tectonophysics 340 (3–4), 195–213.
Sherwin, J.A., Chapple, W.M., 1968. Wavelengths of single layer folds - a Comparison between theory and Observation. American Journal of Science 266 (3), 167–179.
Smith, R.B., 1977. Formation of folds, Boudinage, and Mullions in non-Newtonian materials. Geological Society of America Bulletin 88 (2), 312–320.
Srivastava, D.C., Lisle, R.J., 2004. Rapid analysis of fold shape using Bezier curves. Journal of Structural Geology 26 (9), 1553–1559.
Srivastava, D.C., Rastogi, V., 2010. HingeInflex: a MATLAB-based method for precise selection of the hinge and the inflection points in folds. Geological Magazine 147 (2), 233–241.
Stabler, C.L., 1968. Simplified Fourier analysis of fold shapes. Tectonophysics 6, 343–350.
Turner, F.J., Weiss, L.E., 1963. Structural Analysis of Metamorphic Tectonites. McGraw-Hill, New York, 545 p.
Twiss, R.J., 1988. Description and classification of folds in single surfaces. Journal of Structural Geology 10, 607–623.
Twiss, R.J., Moores, E.M., 2007. Structural Geology. W. H. Freeman and Company, New York, 736 p.
van der Pluijm, B.A., Marshak, S., 2004. Earth Structure. W.W. Norton & Company, New York, 656 p.